Journal of ELECTRONIC MATERIALS, Vol. 47, No. 1, 2018
DOI: 10.1007/s11664-017-5809-x

An Asymmetric Supercapacitor with Mesoporous $NiCo_2O_4$ Nanorod/Graphene Composite and N-Doped Graphene Electrodes

J.W. MAO,[1] C.H. HE,[2] J.Q. QI,[1,3] A.B. ZHANG,[1] Y.W. SUI,[1] Y.Z. HE,[1] Q.K. MENG,[1] and F.X. WEI[1]

1.—School of Materials Science and Engineering, China University of Mining and Technology, Xuzhou 221116, People's Republic of China. 2.—China Zhongyuan Engineering Corp., LTD, Shanghai 100191, People's Republic of China. 3.—e-mail: flower_cumt@outlook.com

In the present work, mesoporous $NiCo_2O_4$ nanorod/graphene oxide ($NiCo_2O_4$/GO) composite was prepared by a facile and cost-effective hydrothermal method and meanwhile, N-doped graphene (N-G) was fabricated also by a hydrothermal synthesis process. $NiCo_2O_4$/GO composite and N-G were used as positive and negative electrodes for the supercapacitor, respectively, which all displayed excellent electrochemical performances. The $NiCo_2O_4$/GO composite electrode exhibited a high specific capacitance of 709.7 F g^{-1} at a current density of 1 A g^{-1} and excellent rate capability as well as good cycling performance with 84.7% capacitance retention at 6 A g^{-1} after 3000 cycles. A high-voltage asymmetric supercapacitor (ASC) was successfully fabricated using $NiCo_2O_4$/GO composite and N-G as the positive and negative electrodes, respectively, in 1 M KOH aqueous electrolyte. The ASC delivered a high energy density of 34.4 Wh kg^{-1} at a power density of 800 W kg^{-1} and still maintained 28 Wh kg^{-1} at a power density of 8000 W kg^{-1}. Furthermore, this ASC showed excellent cycling stability with 94.3% specific capacitance retained at 5 A g^{-1} after 5000 cycles. The impressive results can be ascribed to the positive synergistic effects of the two electrodes. Evidently, our work provides useful information for assembling high-performance supercapacitor devices.

Key words: $NiCo_2O_4$ nanorods, graphene, electrochemical performance, asymmetric supercapacitor

INTRODUCTION

As a new type of energy storage and conversion device, supercapacitors can be applied in a wide variety of fields due to their great advantages such as high power density, long cycle life, fast charging-discharging process and small environmental impact.[1,2] According to the charge storage mechanism, there are two types of supercapacitors, which are electrical double-layer capacitors (EDLCs) and pseudocapacitors.[3–5] Ion adsorption and release at the electrode/electrolyte interface is the energy storage mechanism for EDLCs. As for pseudocapacitors, charge storage is based on Faradaic redox reactions between the electrode and electrolyte.[6] As is known, the capacitance and charge storage of supercapacitors largely depend on electrode materials. Carbon-based active materials show typical double-layer capacitance characteristic with excellent cycling stability, while transition-metal oxides, hydroxides and sulfides are often used as pseudocapacitive electrode materials.[7–10] Compared to EDLCs, pseudocapacitors deliver higher capacitance and energy density owing to their reversible redox reactions, but poor cycling stability. Hence, in order to obtain electrode materials with high

(Received May 17, 2017; accepted September 13, 2017; published online September 24, 2017)

capacitance and super cycling performance, numerous efforts have been devoted to the synthesis of nanostructured transition metal oxide/carbon or graphene composites.[11] Thangappan et al.[12] indicated that compared to pure MoS_2, MoS_2/graphene composite showed higher specific capacitance and superior cycling performance due to interconnected conductive network of the composite and synergetic effect of the two materials.

In recent years, spinel $NiCo_2O_4$, as a very promising electrode material, has attracted wide attention because of its low cost, abundance and environmental friendliness.[13,14] Chen et al.[15] prepared pine-like $NiCo_2O_4$ arrays via a simple hydrothermal method with excellent electrochemical performance. Yuan et al.[16] reported $NiCo_2O_4$ nanosheets on nickel foam via electrodeposition, showing ultrahigh specific capacitance of 1450 F g^{-1} at a current density of 20 A g^{-1} and excellent cycling performance. $NiCo_2O_4$ nanoneedles on nickel foam were obtained by Liu et al.,[17] exhibiting high specific capacitance of 2193 F g^{-1} at 1 A g^{-1} but low cycling performance of 72% retention after 2000 cycles. Graphene, a one-atom-thick sheet of sp^2-bonded carbon atoms in a honeycomb crystal lattice, is noteworthy for its excellent electronic conductivity, high theoretical surface area of 2630 m^2 g^{-1} and good mechanical properties. Graphene has been widely used as a conducting additive for nanostructured composite materials.[18,19] $NiCo_2O_4$/graphene ($NiCo_2O_4$/GO) composite has been reported widely in published papers.[17,20] Generally, grephene is used as a growth substrate for $NiCo_2O_4$, which can display nanoparticle, nanoflower and nanosheet shapes.[21–24] It should be noted that these kinds of composites cannot be fabricated via cost-effective methods and, more importantly, the composites are not suitable for large-scale production.

In this work, $NiCo_2O_4$/GO composite power was obtained via a simple and cost-effective hydrothermal method followed by calcinations. Meanwhile, N-doped graphene (N-G) was also fabricated through a hydrothermal process. An asymmetric supercapacitor (ASC) based on $NiCo_2O_4$/GO composite and N-G was designed. The electrochemical performances of $NiCo_2O_4$/GO and N-G electrodes as well as the ASC have been evaluated. The ASC delivered a maximum energy density of 34.4 Wh kg^{-1} at a voltage of 1.6 V.

EXPERIMENTAL SECTION

Preparation of $NiCo_2O_4$/Graphene Oxide Composite and N-Doped Graphene

All chemicals used in this experiment were of analytical grade and needed no further purification. Graphene oxide (GO) was produced by a modified Hummer's method. The synthesis of $NiCo_2O_4$/GO composite was carried out by a hydrothermal method and annealing. In a typical experiment, 1 mmol of $Ni(NO_3)_2{\cdot}6H_2O$ and 2 mmol of $Co(NO_3)_2{\cdot}6H_2O$ are dissolved in 20 mL of deionized water and then pink solution was obtained. Next, 10 mmol urea was added to the above solution, which was put on a magnetic stirrer and stirred for 30 min to gain well-distributed solution. After that, 12 ml of GO dispersion (2 mg/mL), which had been ultrasonically broken for 4 h, was mixed with the above solution. And this mixed solution was broken by ultrasonic vibration for another 20 min, which was subsequently transferred into a Teflon-lined stainless steel autoclave (50 ml in volume) and heated in an oven at 140°C for 12 h. Then, reaction solution was centrifuged (8000 r/min) in deionized water and anhydrous ethanol to separate $NiCo_2O_4$/GO composite precursor, which was dried in a vacuum at 70°C for 12 h. After that, the dried precipitate was calcinated at 300°C for 3 h in air at a heating rate of 1°C min^{-1} to obtain the final composite material of $NiCo_2O_4$/GO composite. In the obtained $NiCo_2O_4$/GO composite, the theoretical weight ratio of GO and $NiCo_2O_4$ was about 1:10.

The preparation of N-G is similar to that reported in a previous paper.[25] Briefly, GO and urea at a mass ratio of 1:30 were mixed in a beaker. The mixed solution was broken in ultrasound equipment for 1 h, and then transferred into Teflon-lined autoclave and heated at 180°C for 5 h. At high temperature, GO was subjected to the hydrothermal reduction and N-doped reduced GO was formed, which was used as negative material of GCD in this work.

Materials Characterization

The phase structure of $NiCo_2O_4$/GO composite and N-G was identified by x-ray diffraction (XRD, D8 Advance, Bruker, Germany). Field emission scanning electron microscopy (FESEM, Hitachi SU-8000) and high resolution transmission electron microscopy (HRTEM, FEI Tecnai G2 F20) was used to examine the morphologies of $NiCo_2O_4$/GO composite and N-G.

Electrochemical Measurements

The electrochemical performance of $NiCo_2O_4$/GO composite electrode was evaluated in a typical three-electrode configuration in a CHI660E electrochemical workstation (Chenhua, Shanghai). In this system, the obtained specimen, Pt foil and a saturated calomel electrode were used as working electrode, counter electrode and reference electrode, respectively. 1 M KOH solution was employed for electrolyte. Cyclic voltammetry (CV) tests were performed in the potential window of −0.1 V to 0.6 V at the scan rates of 10–50 mV s^{-1}. Galvanostatic charge-discharge (GCD) measurements were conducted at current densities of 1–10 A g^{-1}. The electrochemical impedance spectra (EIS) were measured in the frequency range from 100 kHz to 0.01 Hz with 5 mV amplitude at open circuit potential in the same electrochemical workstation. In

addition, the electrochemical performance of N-G electrode was also evaluated in three-electrode system.

In order to assess the electrochemical performance (CV, GCD, EIS and cycling stability) of $NiCo_2O_4$/GO composite electrode in two-electrode cell, an aqueous ASC was assembled, in which $NiCo_2O_4$/GO composite was used as for positive electrode and N-G for negative electrode.

The specific capacitance (C) of the obtained specimen in three-electrode cell and ASC was calculated from the GCD curves based on Eq. 1 and the power density (P) and energy density (E) of the ASC were obtained according to Eqs. 2 and 3:

$$C = \frac{It}{m\Delta V} \quad (1)$$

$$E = \frac{1}{2}C\Delta V^2 \quad (2)$$

$$P = \frac{E}{t} \quad (3)$$

where I is the constant discharge current, t is the discharge time, m is the mass of active material and ΔV is the potential drop during discharge.

RESULTS AND DISCUSSION

Phase Identification of $NiCo_2O_4$/GO Composite and N-G

The crystal phase and structure information of the as-prepared products were analysized by XRD. Figure 1 presents the XRD patterns of $NiCo_2O_4$/GO composite and N-G. For $NiCo_2O_4$/GO composite, it can be seen that the diffraction peaks at 19.0°, 31.1°, 36.7°, 38.4°, 44.6°, 55.4°, 59.0°, and 65.0° can be indexed as the (111), (220), (311), (222), (400), (422), (511), and (440) planes of cubic $NiCo_2O_4$ phase (JPCDS No. 20-0781). The diffraction peaks of GO cannot be detected in this sample in the XRD, which is perhaps related to its low content, disordered stacking and uniform dispersion in the composite.[26] The XRD pattern of N-doped reduced GO (N-G) is dominated by a very broad diffraction peak at 23.2° (corresponding to its plane spacing of 3.7 nm), which is similar with the feature of reduced GO.[27]

Structure of $NiCo_2O_4$/GO Composite and N-G

Figure 2 reveals the morphology of the as-prepared $NiCo_2O_4$/GO composite at different magnifications. It can be clearly seen in Fig. 2a that $NiCo_2O_4$ nanorods distributed densely on the surface of GO sheets. The magnified image (Fig. 2b) revealed that $NiCo_2O_4$ nanorods were highly mesoporous with a diameter of about 30 nm, which can be ascribed to the release of CO_2 gas during the thermal decomposition process.[28] There is no doubt that this kind of structure can increase the contact area between electrolyte and active material and provide more chance for electrolyte ions accessing the inner realm of active materials, favoring the enhancement of the electrochemical performance of the as-prepared product.[17,29]

In order to further investigate the structure of $NiCo_2O_4$/GO composite and N-G, transmission electron microscopy (TEM) measurement was employed, as shown in Fig. 3. Mesoporous $NiCo_2O_4$ nanorods can also be seen clearly from Fig. 3a, which is in good agreement with the scanning electron microscopy (SEM) results in Fig. 2a. The obvious lattice fringes with interplanar spacing of 0.47 nm and 0.28 nm matched well with the (111) and (220) planes of cubic $NiCo_2O_4$,[17] as shown in Fig. 3b. Figure 3c shows that the as-prepared N-G exhibited a crumpled morphology, composed of a large number of transparent membranes. Similar results have been widely reported in published work.[27,30]

Electrochemical Properties of $NiCo_2O_4$/GO Composite and N-G Electrodes

To evaluate the electrochemical performance of $NiCo_2O_4$/GO composite and N-G, cyclic voltammetry (CV), galvanostatic charge-discharge (GCD), electrochemical impedance spectroscopy (EIS) and cycling stability were tested in a standard three-electrode system, as shown in Fig. 4. Figure 4a displays the CV curves of a $NiCo_2O_4$/GO composite electrode at various scan rates from 10 m s^{-1} to 50 m s^{-1} in the potential window of −0.2 V to 0.5 V [versus a saturated calomel electrode (SCE)]. It is observed that all the CV curves consist of a pair of symmetrical redox peaks, revealing its pseudocapacitance characteristic derived from Faradaic redox reactions of M–O/M–O–OH (M represents Ni and Co in $NiCo_2O_4$) and OH^- in KOH electrolyte.[31] The corresponding reversible reactions are as follows[32,33]:

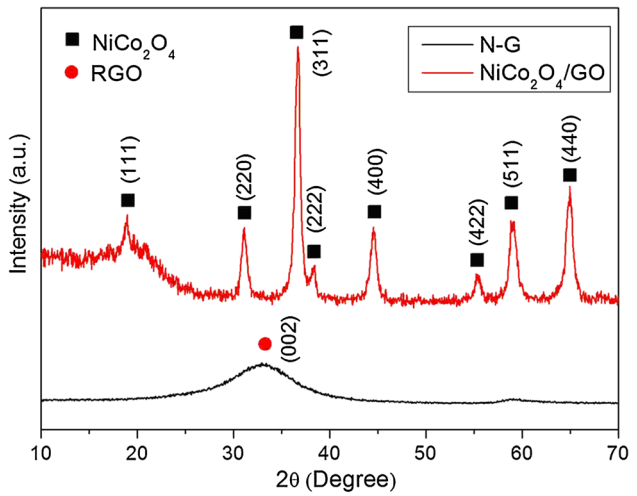

Fig. 1. XRD patterns of $NiCo_2O_4$/GO composite and N-G.

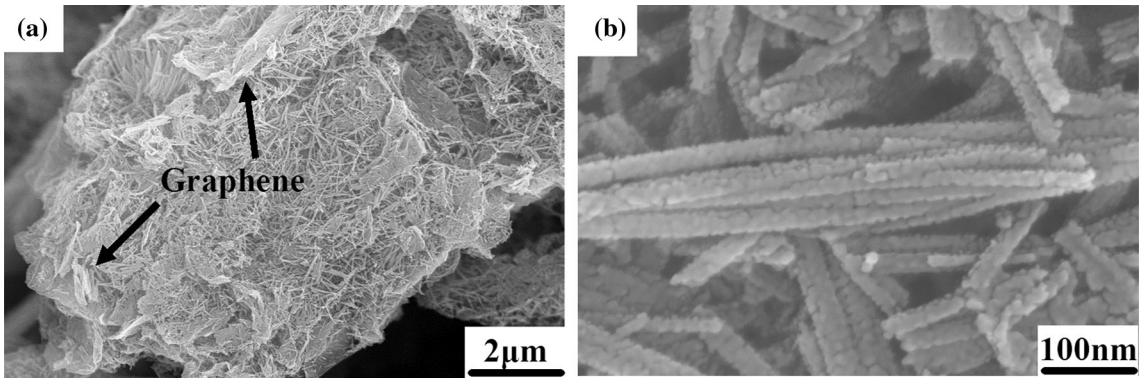

Fig. 2. (a, b) SEM images showing the shape of $NiCo_2O_4$/GO composite at different magnifications.

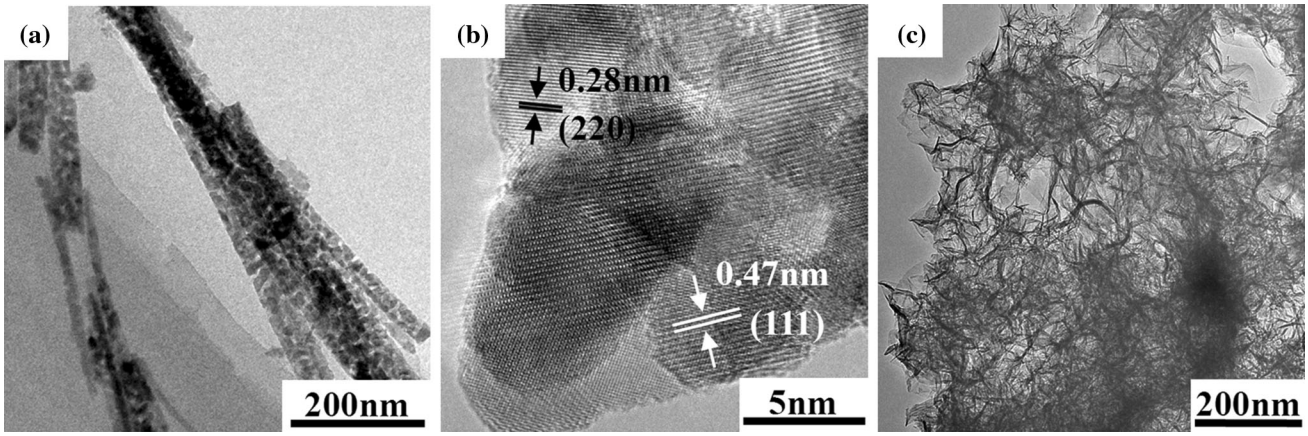

Fig. 3. (a) TEM and (b) high-resolution TEM (HRTEM) images showing $NiCo_2O_4$ nanorods in $NiCo_2O_4$/GO composite. (c) TEM image of N-G.

$$NiCo_2O_4 + OH^- + H_2O \leftrightarrow NiOOH + 2CoOOH + e^- \quad (4)$$

$$CoOOH + OH^- \leftrightarrow CoO_2 + H_2O + e^- \quad (5)$$

This feature is different from that of EDLCs that usually show a rectangular-shaped CV curve. The peak observed around 0.36 V (versus the SCE) at the scan rate of 5 mV s^{-1} is related to the oxidation process (see Eqs. 4 and 5), whereas the peak occurring around 0.15 V corresponds to reduction reaction. The symmetric characteristics of the oxidation and reduction peaks indicates the excellent reversibility of the composite electrode. With the increase of scan rate, the oxidation and reduction peaks increase correspondingly and shift to the positive and negative current directions, respectively, which reflects the variation of the internal resistance of the electrode. Moreover, the shape of every curve remains almost unchanged as the scan rate is increased from 10 mV s^{-1} to 50 mV s^{-1}, meaning enhanced mass transportation and good electron conduction.

GCD testing was performed on the same electrode at different current densities in the voltage range of 0–0.5 V (versus the SCE) to gain the specific capacitance (Fig. 4b). It can be clearly seen that each curve exhibits a discharge plateau, owing to the Faradaic reactions and corresponding to the redox peaks in the CV curves (Fig. 4a). The calculated specific capacitances of the $NiCo_2O_4$/GO composite electrode are shown in Fig. 4c, which are 709.7 F g^{-1}, 700.8 F g^{-1}, 629.3 F g^{-1}, 585.3 F g^{-1}, 556.4 F g^{-1}, and 535.6 F g^{-1} at current densities of 1 A g^{-1}, 2 A g^{-1}, 4 A g^{-1}, 6 A g^{-1}, 8 A g^{-1}, and 10 A g^{-1}, respectively.

As the current density increases to 10 A g^{-1}, 75.5% of its initial specific capacitance is retained. The decrease of specific capacitance with current density can be ascribed to the diffusion effect limiting the diffusion of the electrolyte ions at high current density, resulting in the low utilization of active material.

From the viewpoint of practical application, cycling stability is a critical factor for supercapacitors, which was measured via repeated charging-discharging processes at 6 A g^{-1}, as illustrated in Fig. 4d. It is observed that the capacity decreases gradually with the increasing number of cycles. After 3000 cycles, the specific capacitance reduces to 496 F g^{-1} and 84.7% of its initial capacity is retained, indicating the good cycling performance.

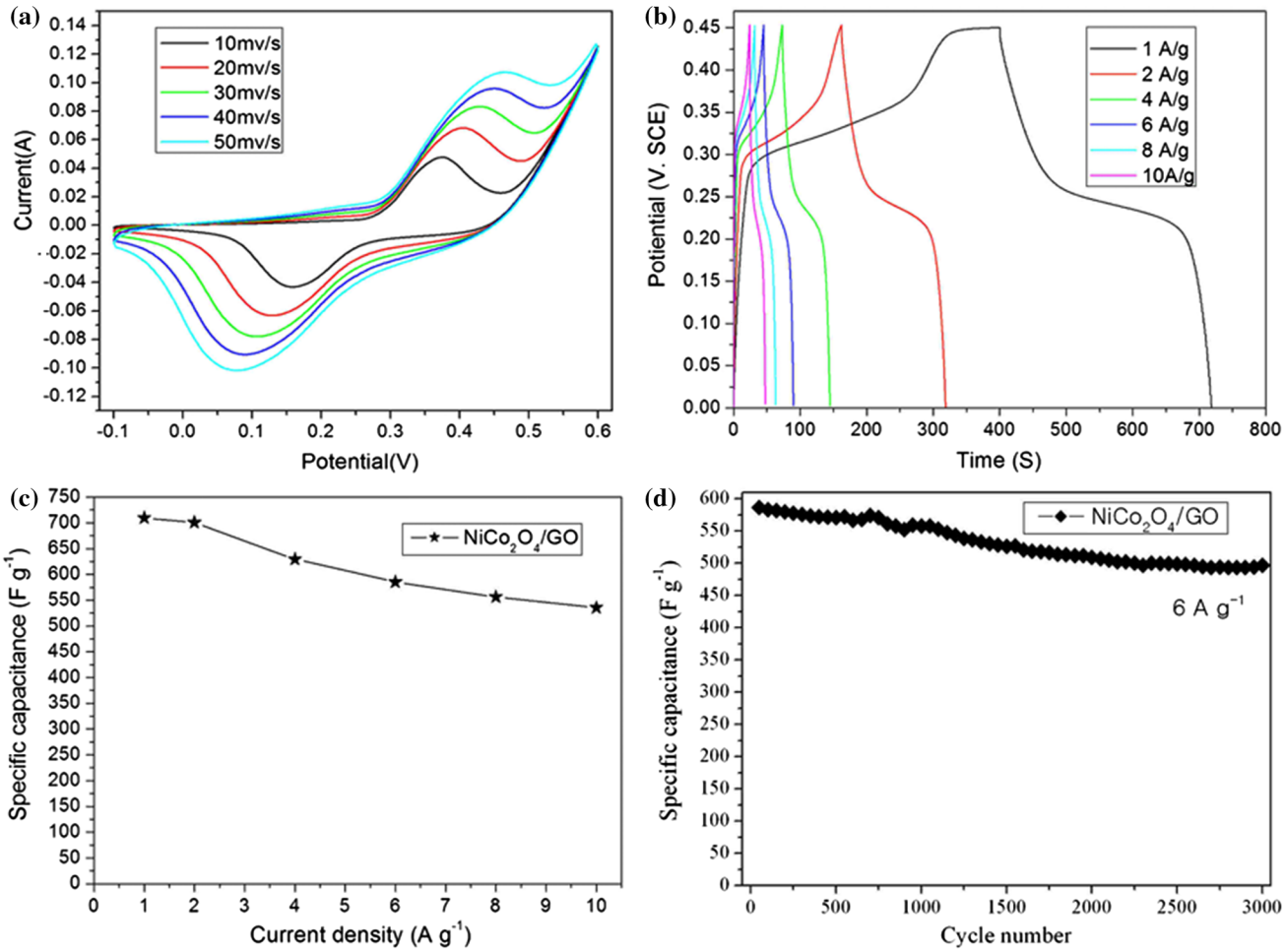

Fig. 4. (a) Cyclic voltammetry (CV) curves of $NiCo_2O_4$/GO composite electrode, (b) galvanostatic charge-discharge (GCD) curves of $NiCo_2O_4$/GO composite electrode, (c) specific capacitance as a function of current density and (d) cycling performance of $NiCo_2O_4$/GO composite at a current density of 6 A g^{-1}.

This may be attributed to the following two reasons: graphene sheets in the composite can buffer the volume change of $NiCo_2O_4$ during the charge-discharge process; graphene sheets enhance the electrical conductivity of the composite.

EIS analysis was carried out to further investigate the electrochemical performance of this electrode. Figure 5 shows Nyquist plot of a $NiCo_2O_4$/GO composite electrode in the frequency range from 10 kHz to 0.01 Hz. The impedance spectra consist of a linear low-frequency region and a quasi-semicircle high-frequency part. The linear region is associated with the Warburg impedance, reflects the kinetics of the electrolyte diffusion to the electrode's surface.[34] The Warburg angle is close to 56°, meaning easy electrolyte diffusion to the electrode's surface.[35] In the high-frequency region, charge transfer impendence (Rct) and equivalent series resistance (Rs) correspond to the semicircle and intersection with the real axis, respectively.[21,36] According to the inset in Fig. 5, the values of Rs and Rct are 0.12 and 0.42 O, respectively, which are lower than those reported in previous work.[36,37] The low values of Rs

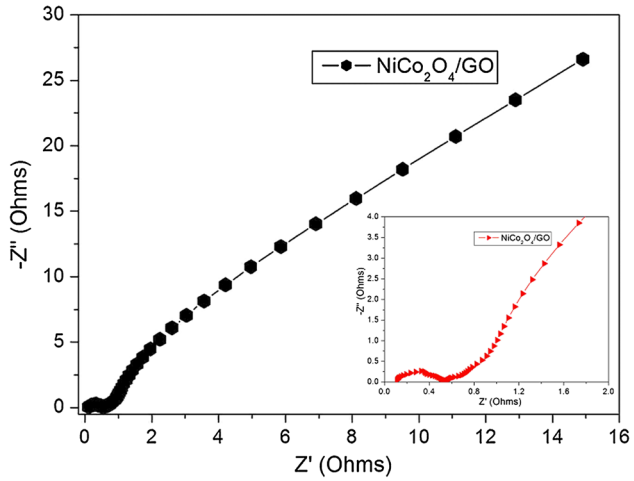

Fig. 5. Nyquist plot of a $NiCo_2O_4$/GO composite electrode at open circuit potential. The inset is the enlarged plot of the high-frequency region.

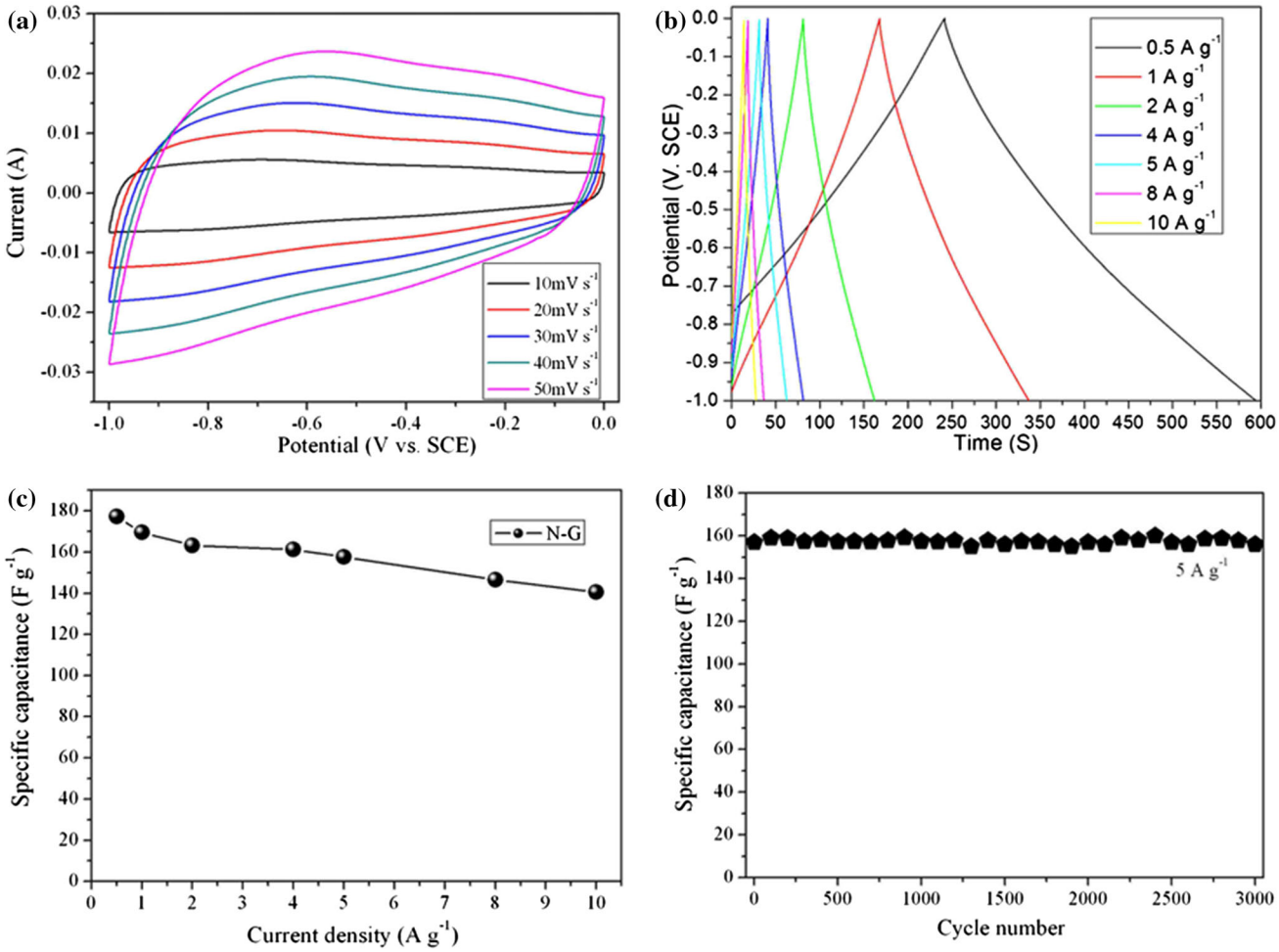

Fig. 6. (a) CV curves of an N-G electrode over a potential widow of −1 V to 0 V at various scan rates, (b) GCD curves of an N-G electrode from 0.5 A g^{-1} to 10 A g^{-1}. (c) Relationship between specific capacitance and current density and (d) cycling performance of an N-G electrode at 5 A g^{-1}.

and Rct reflect the good electrical contact between $NiCo_2O_4$/GO composite and N-G and high conductivity of this material.[34,38] Clearly, these features ascribe to the high rate capability and super cycling performance of the $NiCo_2O_4$/GO composite electrode.

The electrochemical properties of the N-G electrode are illustrated in Fig. 6. Figure 6a shows the CVs of this electrode at different scan rates with potential window of −1 V to 0 V. Rectangular-shaped CV curves without obvious distortion even at a high scan rate can be observed in Fig. 6a, indicating its ideal EDLC nature during the charge-discharge process and reflecting the fast diffusion of electrolyte ions into the N-G electrode. GCD curves of the N-G electrode are presented in Fig. 6b; they are all linear and symmetrical even at high current density. This also reflects the EDLC feature of an N-G electrode. The specific capacitances of the N-G electrode calculated from GCD curves are 177.2 F g^{-1}, 169.5 F g^{-1}, 163.2 F g^{-1}, 161.3 F g^{-1}, 157.6 F g^{-1}, 146.6 F g^{-1}, and 140.5 F g^{-1} at current densities of 0.5 A g^{-1}, 1 A g^{-1}, 2 A g^{-1}, 4 A g^{-1}, 5 A g^{-1}, 8 A g^{-1}, and 10 A g^{-1}, respectively, as shown in Fig. 6c, showing high rate capability. After 3000 cycles, capacitance retention of the N-G electrode can reach 100% (see Fig. 6d), indicating its excellent cycling stability. These outstanding results demonstrate that N-G has great potential for negative electrode material in supercapacitors.

Electrochemical Properties of $NiCo_2O_4$/GO// N-G Asymmetric Supercapacitor

As reported, $NiCo_2O_4$ and its composite with high electrochemical performance have been developed for positive electrode materials in ASCs with high energy density.[39–41] An aqueous-based ASC was designed using $NiCo_2O_4$/GO composite as positive electrode and N-G as negative electrode material in 1 M KOH electrolyte. The electrochemical performance of the $NiCo_2O_4$/GO//N-G ASC was characterized by CV, GCD, EIS and cycling life. To obtain good electrochemical performance for the $NiCo_2O_4$/GO//N-G ASC, positive and negative electrodes

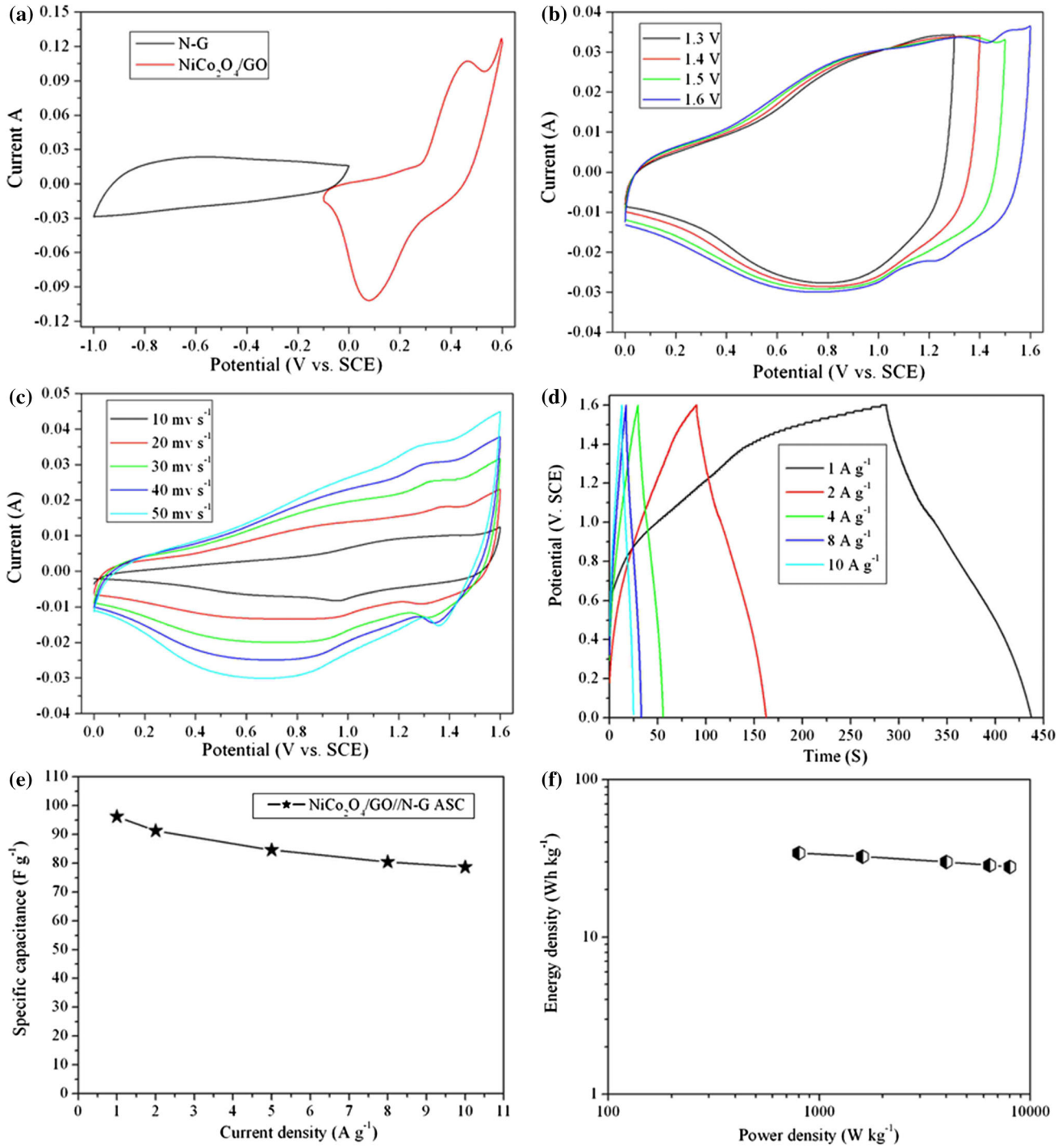

Fig. 7. (a) CV comparison of $NiCo_2O_4$/GO and N-G electrodes at different potential windows in 1 M KOH solution, (b) CV curves of $NiCo_2O_4$/GO//N-G ASC at different potential windows, (c) CV curves of the ASC at different scan rates, (d) GCD curves of the ASC at various current densities, (e) specific capacitance as a function of current density and (f) the relationship between energy density and power density.

should satisfy the charge balance. According to the specific capacitances and potential windows of $NiCo_2O_4$/GO composite and N-G, the optimal mass ratio between the positive and negative active materials should be 0.53 for a $NiCo_2O_4$/GO//N-G ASC cell.

Figure 7a compares the CV curves of $NiCo_2O_4$/GO composite and N-G electrodes at a scan rate of 50 mV s^{-1} in the three-electrode system. It can be observed that these two materials have different potential ranges. It presents the CV curves of the $NiCo_2O_4$/GO composite within a voltage window of

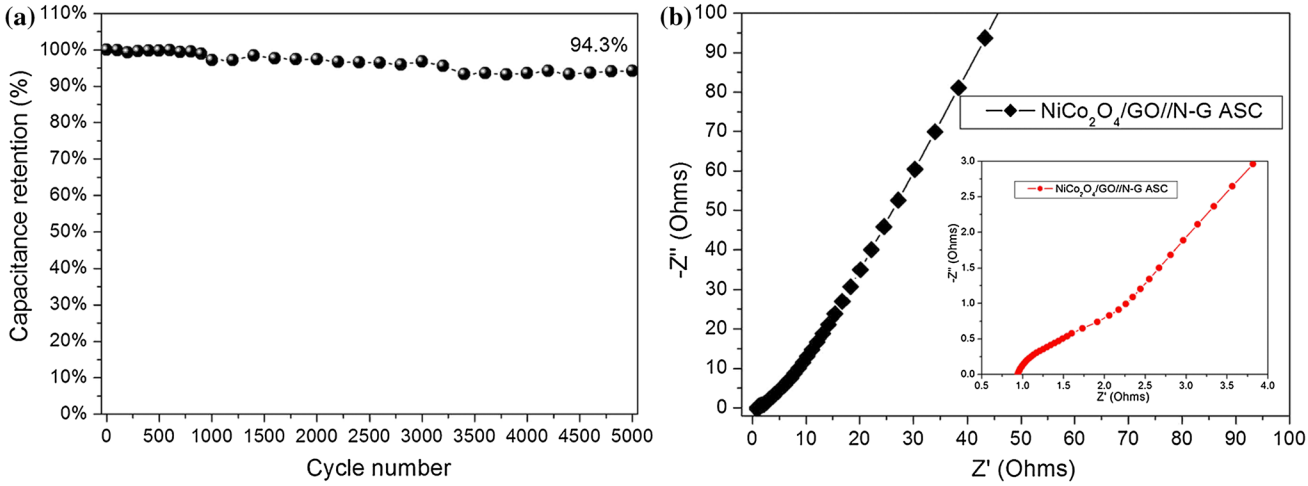

Fig. 8. (a) Long-term cycling performance of a $NiCo_2O_4$/GO//N-G ASC and (b) Nyquist plot of the ASC; the inset shows the enlarged plot of the high-frequency region.

−0.1 V to 0.6 V (versus an SCE) and the N-G electrode within a voltage window of −1 V to 0 V. The former exhibits a pair of redox peaks, whereas the latter shows a nearly rectangular shape. The obvious difference is due to the fact that the capacitance of $NiCo_2O_4$/GO composite comes from the redox pseudocapacitance of $NiCo_2O_4$ and electrical double-layer capacitance of graphene in this composite. But the capacitance of N-G only derives from the contribution of electrical double-layer.

If the total cell voltage is the sum of the potential ranges of $NiCo_2O_4$/GO composite and N-G, the total cell voltage may be extended up to 1.6 V in 1 M KOH aqueous solution for $NiCo_2O_4$/GO//N-G ASC. Figure 7b exhibits the CV curves of $NiCo_2O_4$/GO//N-G ASC at different voltage windows of 1.3–1.6 V at a scan rate of 50 mV s^{-1}. It is observed that the $NiCo_2O_4$/GO//N-G ASC shows a stable capacitive behavior with the features of both pseudocapacitive and an EDLC even at the potential window up to 1.6 V since the redox peaks reflect the pseudocapacitive property of the ASC. This also shows that pseudocapacitance and electrical double-layer capacitance all contribute to the capacitance of $NiCo_2O_4$/GO//N-G ASC. Similar results have been reported in a previous article.[26]

CV curves of the ASC with a potential window of 0–1.6 V at various scan rates of 10 mV s^{-1}, 20 mV s^{-1}, 30 mV s^{-1}, 40 mV s^{-1}, and 50 mV s^{-1} in 1 M KOH aqueous electrolyte are shown in Fig. 7c. With the increase of scan rate, severe Faradaic reactions happen. In addition, the shape of CV curves can be well maintained, confirming the efficient charge storage behavior. As shown in Fig. 7d, GCD testing was conducted at various current densities ranging from 1 A g^{-1} to 10 A g^{-1} to further examine the electrochemical performance. Based on Eq. 1, $NiCo_2O_4$/GO//N-G ASC delivers specific capacitances of 96.2 F g^{-1}, 91.3 F g^{-1}, 84.6 F g^{-1}, 80.5 F g^{-1}, and 78.7 F g^{-1} at current densities of 1 A g^{-1}, 2 A g^{-1}, 5 A g^{-1}, 8 A g^{-1}, and 10 A g^{-1}, respectively, as shown in Fig. 7e. Evidently, the ASC exhibits a high rate performance of 82%.

Power density (P) and energy density (E) are the two key parameters for estimating the performance of supercapacitors, and are calculated according to Eqs. 2 and 3, respectively. $NiCo_2O_4$/GO//N-G ASC possesses an energy density of 34.4 Wh kg^{-1} at a power density of 800 W kg^{-1} and still maintains 28 Wh kg^{-1} at a power density of 8000 W kg^{-1} (Fig. 7f). This energy density is higher than that of other symmetrical supercapacitors, such as MoS_2/GF// activated carbon,[42] sulfonated polyaniline functionalized reduced GO//RGO,[43] IL-CNT-graphene gel// MnO_2-graphene gel,[44] MnO_2/$MnCO_3$/rGO//rGO,[45] GF/CNT/MnO2 and GF/CNT/Ppy hybrid films[46] and N-doped carbon//NiO.[47] The high-energy density of the ASC can be reasonably ascribed to the synergistic effect of $NiCo_2O_4$/GO composite and N-G, i.e., high specific capacitance of the two electrodes and wide potential window.

Long-term cycling life is also an important parameter for supercapacitor devices. Figure 8a displays the cycling performance of a $NiCo_2O_4$/GO//N-G ASC charged at 1.6 V at 5 A g^{-1}. After 5000 cycles, the specific capacitance of the ASC reduces slightly from 84.6 F g^{-1} to 79.8 F g^{-1}, indicating the excellent cycling stability of $NiCo_2O_4$/GO//N-G ASC with 94.3% capacitance retention. The Nyquist plot of the ASC at open-circuit voltage is shown in Fig. 8b; it is also composed of a linear part and a quasi-semicircle. The calculated values of Rs and Rct are 0.93 O and 0.72 O, respectively. The slope in the lower-frequency region is about 68°, meaning the low diffusive resistance of the electrolyte in the ASC.[35] These factors favor the enhancement of rate capability and cycling stability of a $NiCo_2O_4$/GO//N-G ASC.

CONCLUSION

In summary, $NiCo_2O_4$ nanorod/graphene composite ($NiCo_2O_4$/GO) was fabricated by a facile and cost-effective hydrothermal method followed by calcination. Meanwhile, N-G was also prepared via a hydrothermal process. $NiCo_2O_4$/GO composite and N-G electrodes all exhibited excellent electrochemical performances. The $NiCo_2O_4$/GO composite electrode delivered a high specific capacitance of 709.7 F g^{-1} at a current density of 1 A g^{-1} and good cycling stability with 84.7% capacitance retention at 6 A g^{-1} after 3000 cycles. The N-G electrode showed high rate capability and excellent cycling performance. An ASC was designed using $NiCo_2O_4$/GO composite and N-G as positive and negative electrodes, respectively, in 1 M KOH aqueous electrolyte, exhibiting a high-energy density of 34.4 Wh kg^{-1} at a power density of 800 W kg^{-1} along with super cycling stablity of 94.3% retention at 5 A g^{-1} after 5000 cycles. It is believed that the ASC prepared by this strategy with low cost has great prospective application in energy storage devices.

ACKNOWLEDGEMENTS

This work was financially supported by the Fundamental Research Funds for the Central Universities (No. 2017XKQY005).

REFERENCES

1. Y. Gogotsi and P. Simon, *Science* 334, 917 (2011).
2. Q. Wang, J. Yan, and Z.J. Fan, *Energy Environ. Sci.* 9, 729 (2016).
3. J. Ye, Z. Li, Z. Dai, Z.Y. Zhang, M.Q. Guo, and X.J. Wang, *J. Electron. Mater.* 45, 4237 (2016).
4. L.Y. Jiang, Y.W. Sui, J.Q. Qi, Y. Chang, Y.Z. He, Q.K. Meng, F.X. Wei, Z. Sun, and Y.X. Jin, *Part. Part. Syst. Charact.* 34, 1600239 (2017).
5. I.S. Ike, I. Sigalas, and S.E. Iyuke, *J. Electron. Mater.* 46, 1163 (2017).
6. B. Li, F. Dai, Q.F. Xiao, L. Yang, J.M. Shen, C.M. Zhang, and M. Cai, *Energy Environ. Sci.* 9, 102 (2016).
7. S. Maiti, A. Pramanik, and S. Mahanty, *Acs Appl. Mater. Inter.* 6, 10754 (2014).
8. Z.C. Li, J. Han, L. Fan, M.G. Wang, S.Y. Tao, and R. Guo, *Chem. Commun.* 51, 3053 (2015).
9. Y. Chang, Y.W. Sui, J.Q. Qi, L.Y. Jiang, Y.Z. He, F.X. Wei, Q.K. Meng, and Y.X. Jin, *Electrochim. Acta* 226, 69 (2017).
10. M. Mandal, D. Ghosh, K. Chattopadhyay, and C.K. Das, *J. Electron. Mater.* 45, 3491 (2016).
11. C.J. Yuan, H.B. Lin, H.Y. Lu, E.D. Xing, Y.S. Zhang, and B.Y. Xie, *Appl. Energy* 178, 260 (2016).
12. R. Thangappan, S. Kalaiselvam, A. Elayaperumal, R. Jayavel, M. Arivanandhan, R. Karthikeyan, and Y. Hayakawa, *Dalton Trans.* 45, 2637 (2016).
13. A. Ramadoss, K.N. Kang, H.J. Ahn, S.I. Kim, S.T. Ryu, and J.H. Jang, *J. Mater. Chem. A* 4, 4718 (2016).
14. C.R. Zheng, C.B. Cao, R.L. Chang, J.H. Hou, and H.Z. Zhai, *Phys. Chem. Chem. Phys.* 18, 6268 (2016).
15. Y.J. Chen, B.H. Qu, L.L. Hu, Z. Xu, Q.H. Li, and T.H. Wang, *Nanoscale* 5, 9812 (2013).
16. C.Z. Yuan, J.Y. Li, L.R. Hou, X.G. Zhang, L.F. Shen, and X.W. Lou, *Adv. Funct. Mater.* 22, 4592 (2012).
17. S.N. Liu, J. Wu, J. Zhou, G.Z. Fang, and S.Q. Liang, *Electrochim. Acta* 176, 1 (2015).
18. Y. Chang, Y.W. Sui, J.Q. Qi, L. Jiang, Y.Z. He, F.X. Wei, Q.K. Meng, and Y.X. Jin, *Electrochim. Acta* 226, 69 (2017).
19. S. Kirchhecker, M. Antonietti, and D. Esposito, *Green Chem.* 16, 3705 (2014).
20. A.C. Mtukula, J. Shen, X.J. Bo, and L.P. Guo, *J. Alloy. Compd.* 655, 229 (2016).
21. V.H. Nguyen and J.J. Shim, *J. Power Sources* 273, 110 (2015).
22. J. Zhou, Y. Huang, X.H. Cao, B. Ouyang, W.P. Sun, C.L. Tan, Y. Zhang, Q.L. Ma, S.Q. Liang, Q.Y. Yan, and H. Zhang, *Nanoscale* 7, 7035 (2015).
23. C. Zhang, T. Kuila, N.H. Kim, S.H. Lee, and J.H. Lee, *Carbon* 89, 328 (2015).
24. H.W. Wang, Z.A. Hu, Y.Q. Chang, Y.L. Chen, H.Y. Wu, Z.Y. Zhang, and Y.Y. Yang, *J. Mater. Chem.* 21, 10504 (2011).
25. H.L. Guo, P. Su, X.F. Kang, and S.K. Ning, *J. Mater. Chem. A* 1, 2248 (2013).
26. J. Yan, Z.J. Fan, W. Sun, G.Q. Ning, T. Wei, Q. Zhang, R.F. Zhang, L.J. Zhi, and F. Wei, *Adv. Funct. Mater.* 22, 2632 (2012).
27. Z.L. Ma, X.B. Huang, S. Dou, J.H. Wu, and S.Y. Wang, *J. Phys. Chem. C* 118, 17231 (2014).
28. J.P. Wang, S.L. Wang, Z.C. Huang, and Y.M. Yu, *J. Mater. Chem. A* 2, 17595 (2014).
29. D.Z. Kong, C.W. Cheng, Y. Wang, J.I. Wong, Y.P. Yang, and H.Y. Yang, *J. Mater. Chem. A* 3, 16150 (2015).
30. Z. Gao, W.L. Yang, J. Wang, N.N. Song, and X.D. Li, *Nano Energy* 13, 306 (2015).
31. G.X. Gao, H.B. Wu, S.J. Ding, L.M. Liu, and X.W. Lou, *Small* 11, 804 (2015).
32. N. Padmanathan and S. Selladurai, *Ionics* 19, 1535 (2013).
33. Y.R. Zhu, X.L. Pu, W.X. Song, Z.B. Wu, Z. Zhou, X. He, F. Lu, M.J. Jing, B. Tang, and X.B. Ji, *J. Alloy. Compd.* 617, 988 (2014).
34. J. Wu, R. Mi, S. Li, P. Guo, J. Mei, H. Liu, W.M. Lau, and L.M. Liu, *Rsc Adv.* 5, 25304 (2015).
35. Q. Yang, Z.Y. Lu, X.M. Sun, and J.F. Liu, *Sci. Rep.* 3, 3537 (2013).
36. R.J. Zou, K.B. Xu, T. Wang, G.J. He, Q. Liu, X.J. Liu, Z.Y. Zhang, and J.Q. Hu, *J. Mater. Chem. A* 1, 8560 (2013).
37. Y.Y. Wei, S.Q. Chen, D.W. Su, B. Sun, J.G. Zhu, and G.X. Wang, *J. Mater. Chem. A* 2, 8103 (2014).
38. T. Zhu, E.R. Koo, and G.W. Ho, *Rsc Adv.* 5, 1697 (2015).
39. A. Shanmugavani and R.K. Selvan, *Electrochim. Acta* 189, 283 (2016).
40. C.T. Hsu and C.C. Hu, *J. Power Sources* 242, 662 (2013).
41. S. Khalid, C.B. Cao, L. Wang, and Y.Q. Zhu, *Sci. Rep.* 6, 22699 (2016).
42. T.M. Masikhwa, M.J. Madito, A. Bello, J.K. Dangbegnon, and N. Manyala, *J. Colloid Interface Sci.* 488, 155 (2017).
43. P. Bandyopadhyay, T. Kuila, J. Balamurugan, T.T. Nguyen, N.H. Kim, and J.H. Lee, *Chem. Eng. J.* 308, 1174 (2017).
44. Y.M. Sun, Y.B. Cheng, K. He, A.J. Zhou, and H.W. Duan, *Rsc Adv.* 5, 10178 (2015).
45. Y.C. Liu, D.W. He, H.L. Wu, J.H. Duan, and Y.N. Zhang, *Electrochim. Acta* 164, 154 (2015).
46. J.L. Liu, L.L. Zhang, H.B. Wu, J.Y. Lin, Z.X. Shen, and X.W. Lou, Energ. *Environ. Sci.* 7, 3709 (2014).
47. G. Qu, S.F. Jia, H. Wang, F. Cao, L. Li, C. Qing, D.M. Sun, B.X. Wang, Y.W. Tang, and J.B. Wang, *Acs Appl. Mater. Inter.* 8, 20822 (2016).